*Nano and Medical Materials 2023; 3(2): 249.*
Original Research Article

# Hydrothermal synthesis of valve metal Zr-doped titanate nanofibers for bone tissue engineering

**Parker Cole[1,†], Yang Tian[2,†], Savannah Thornburgh[3], Mary Malloy[3], Lauren Roeder[3], Micah Maulding[4], Yan Huang[5], Z. Ryan Tian[2,4,*]**

[1] *Biomedical Engineering, and Institute for Nanoscience/Engineering, University of Arkansas, Fayetteville, AR 72701, USA*

[2] *Material Science/Engineering, and Institute for Nanoscience/Engineering, University of Arkansas, Fayetteville, AR 72701, USA*

[3] *Biological Sciences, University of Arkansas, Fayetteville, AR 72701, USA*

[4] *Chemistry and Biochemistry, and Institute for Nanoscience/Engineering, University of Arkansas, Fayetteville, AR 72701, USA*

[5] *Animal Science, University of Arkansas, Fayetteville, AR 72701, USA*

*** Corresponding author:** Z. Ryan Tian, rtian@uark.edu

[†] *These authors equally contributed to this work.*

**ARTICLE INFO**

Received: 7 October 2023
Accepted: 20 October 2023
Available online: 20 November 2023

doi: 10.59400/nmm.v3i2.249



**ABSTRACT:** Investigations are underway to identify novel biomaterials to improve strategies for bone tissue engineering. Hybrid nanomaterials have emerged as a viable class of biomaterials. Here, we report a facile, economical, optimized, and well-controlled hydrothermal method for synthesizing Zr-doped potassium titanate nanofibers with high purity. Upon morphological characterization, Zr-doping did not disrupt the parent crystal structure of potassium titanate, which showed huge potential for bone tissue engineering.

***KEYWORDS:*** nanosynthesis; titanate nanofiber; bone tissue engineering; bone-scaffold; zirconium doping

## 1. Introduction

Nanoparticles have the potential to improve mechanical properties, release therapeutic ions or molecules into the surrounding environment in order to enhance osteoblast cell recruitment, adhesion, proliferation, and differentiation; enhance surface energy and protein adsorption and influence integrin binding; and act as a radiopacifier for enhanced visual detection under X-ray imaging[1–10]. With the emergence of nanotechnology, tissue engineering has seen a wide spectrum of improvements, ranging from architectural design and stability to multifunctional materials.

Since bone is a natural bio-nanocomposite, it has been our goal to create nanoscale mimicry of natural bone using new materials that could enhance bone tissue growth for bone regeneration. Recent studies have shed some new light on understanding and controlling the mechanism(s) behind the pivotal role of nanotechnologies in orthopedic applications. Nanoscale factors such as grain size, pore shape and size, surface roughness and surface area-to-volume ratio, surface wettability, and associated energetics have been attributed to such optimized performance[11]. To this end, a widely expanding range of nanomaterials and nanotechnologies have been developed, investigated, and employed in the field of bone tissue engineering[12–14].

Titanium dioxide has attracted considerable attention since the convergence of orthopedics and

nanomaterial science. This is based largely on the fundamental understanding that Ti metal surfaces oxidize upon contact with air, resulting in a dense layer of native titanium dioxide ($TiO_2$) on the surface. Studies have shown that anodization, a method to controllably form an oxide surface coating, promotes the formation of a biologically compatible and osteogenic surface coating. Enrichments with the help of nanomaterial chemistry have furthered this area of research, and many labs have structurally controlled this $TiO_2$ layer in morphologies such as nanofibers and nanotubes[15–17]. Interestingly, it has also been discovered that some synthetic approaches can give rise to ionic intermediate titanate clusters[18]. This crystal structure has a clay-like lattice comprised of edge-sharing $TiO_6$ octahedra intercalated by cationic species. It is this layered structure that has been found to promote apatite formation in simulated body fluid (SBF)[18]. Powdery $TiO_2$ minerals (e.g., rutile, anatase) hydrothermally react with a water solution of sodium (or potassium) hydroxide, forming the nanotube or nanowire of Na- or K-titanate, depending on the hydrothermal reaction temperature. Thus-formed ionic layered structure provides a cation "reservoir" for potential ion-exchange with cations in the body fluids, which can autonomously in real-time balance the cations in situ to help bone tissue growth. In simulated body fluid (SBF), the Na/K-titanate is in a hypotonic state when compared to the calcium ($Ca^{2+}$) concentration of the SBF. This promotes the ion-exchange of monovalent $Na^+$ or $K^+$ ions for $Ca^{2+}$ in the SBF. Thereafter, a secondary mechanism is evoked—the phosphate（i.e., $(PO_3)^{3-}$, $(HPO_3)^{2-}$, $(H_2PO_3)^-$) anions in body fluid with the titanate surface $Ca^{2+}$—forming hydrated calcium phosphate, a biomineral called hydroxy appetite as a major building block of natural bone, which is critical for an osteogenic/osteoconductive environment[18].

Additionally, doping $TiO_2$ has provided an alternative strategy to hybridize other pro-bone elements (such as other valve metals: Zr, Nb, or Ta) into heterogeneous nanostructures rather than try and develop difficult, or costly, approaches to obtain pure species such as zirconium dioxide ($ZrO_2$, called zirconia)[19–24]. Zirconia-based nanomaterials have been demonstrated to be osteoconductive; however, their syntheses typically require a yttrium stabilization agent and/or have not become commercially viable for large-scale production[25–30].

To help bring new zirconium-doped nanomaterials for orthopedic implants to market, we conducted this nanosynthesis study systematically to assess the feasibility of producing long and pristine nanofibers of zirconium-doped titanate. The doping optimization was confirmed using characterization data from scanning electronic microscopy with an energy-dispersive elemental analyzer (SEM-EDX) together with X-ray diffraction (XRD) and X-ray photoelectron spectroscopy (XPS).

## 2. Materials and methods

### 2.1. Nanofiber synthesis

The Zr-doped potassium titanate nanofibers were prepared following a published protocol[29,30] with some modifications. Briefly, in a Teflon cup containing a 50-mL water solution of 10M KOH, 500 mg of $TiO_2$ powder (Aeroxide P25) was added to the Teflon and stirred for about 5 min with a Teflon-coated magnetic stirring bar on an electrical stirrer. Thereafter, $ZrO_2$ powder (chemical grade, from Johnson Matthey) was mixed with the KOH solution to form a mixture upon stirring. Here, the molar ratio of Zr-dopant to Ti was widely varied, ranging from 1%–5%.

Next, the mixture-containing Teflon cup was sealed in an autoclave container, heated in an oven at 240 °C for 72 h, and then cooled down in the air. The white powdery product was collected, water-washed until pH = 7, and finally air-dried for characterization. To keep the nanofiber lattice intact, it is important to do the water-washing step carefully, as detailed separately below.

### 2.2. Post synthesis washing

The fibers were formed as a slurry from the high-alkalinity environment in the autoclave treatment. To remove the residual KOH, the white slurry went through a well-controlled neutralization process. The nanofiber slurry was first centrifuged for 5 min at 4000 rpm. The supernatant was decanted and then mixed with deionized water to form another slurry with a lower KOH content, which was repeated until the supernatant's pH = 7.

### 2.3. Characterization

The SEM-EDX analysis was carried out on the FEI Nova NanoLab 200 to assess nanofiber morphology and chemical composition. Typically, the fiber sample was placed on an aluminum holder to let the sample dry in the air. Once dried, the holder was placed in a plasma sputtering coater with an Au-target to coat the sample surface with Au. The XRD was performed with the Rigaku MiniFlex II Desktop X-ray diffractometer using monochromatized Cu-Kα (λ = 1.5406 Å) at 30 kV and 15 mA in the range of 2θ from 5° to 60° at a speed of 0.1°/min. to assess crystal structure. The XPS was conducted on the PHI VersaProbe Scanning XPS system to study the chemical environment of Zr.

## 3. Results & discussion

### Zirconium doping

The Zr-doped potassium titanate nanofibers self-assembled into curving sheets upon drying (**Figure 1a**). At higher magnification (**Figure 1b**), the clean and well-crystallized long nanofibers in self-entangled sheets can be clearly seen, which is a characteristic of the Zr-doped potassium titanate nanofibers. The nanofiber length extends into the micron range, whereas the width of these fibers is under 100 nm.

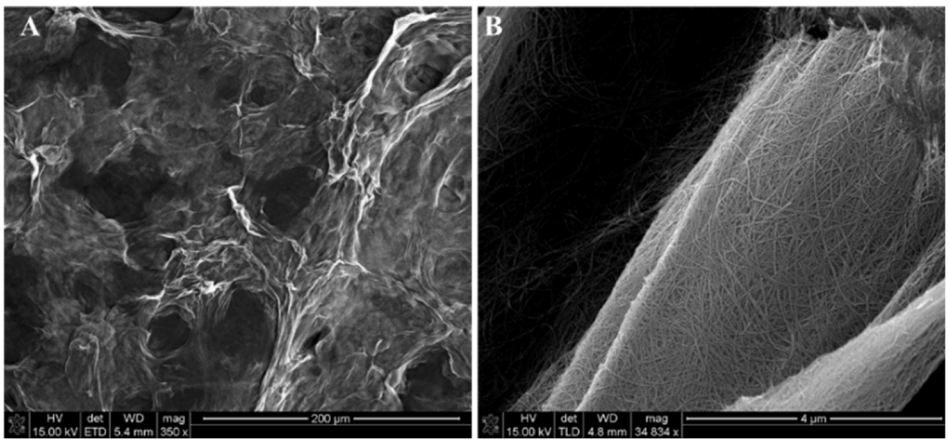


**Figure 1.** SEM micrographs of Zr-doped potassium titanate. **(a)** Scale bar: 200 µm; **(b)** Scale bar: 4 µm.

Additionally, **Figure 1b** shows the relatively smooth surface of the high length-to-width ratio (or aspect ratio) nanofibers, suggesting an optimal control over the nanosynthesis parameters to achieve uniformly distributed Zr-doping throughout the lattice.

On the EDAX map (**Figure 2**), the Zr dopants (red) are distributed along the fiber axis, showing overlap with the Ti species (green), indicating the lattice building blocks of the smaller $TiO_6$ octahedra more than the larger $ZrO_6$ octahedra. Seemingly, the $ZrO_6$ octahedra are well-dispersed, allowing for the structural distortion of each $ZrO_6$ octahedron to not destroy the lattice structural continuity. The high

dispersion of Zr dopant in the nanofiber structure suggests the optimal doping conditions that support **Figure 1**.

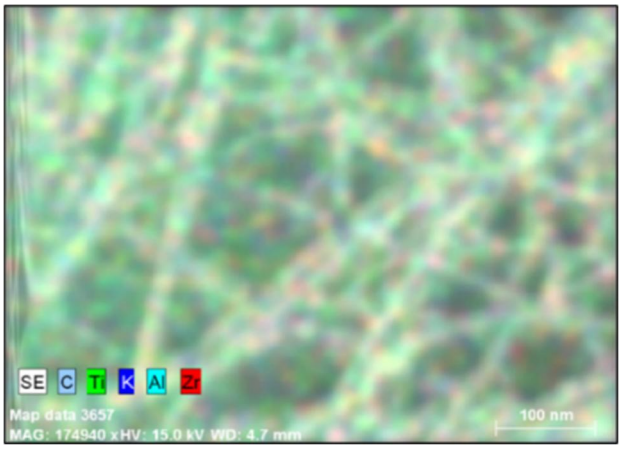


**Figure 2.** Element dispersive EDX mapping of the Zr-doped potassium titanate nanofibers. Scale bar: 100 nm.

The nanofiber crystal structure can be characterized using XRD patterns (**Figure 3**). All the XRD peaks of 200, 310, 403, and 603 can be assigned to the layered $K_2Ti_6O_{13}$ titanate lattice[30]. No residual impurity was detected, as evidenced by no extra peaks in the XRD pattern due to the XRD detection limit, which indicates that the larger $ZrO_6$ octahedron is well-doped in the titanate crystal structure to maintain the lattice integrity and nanofiber structure.

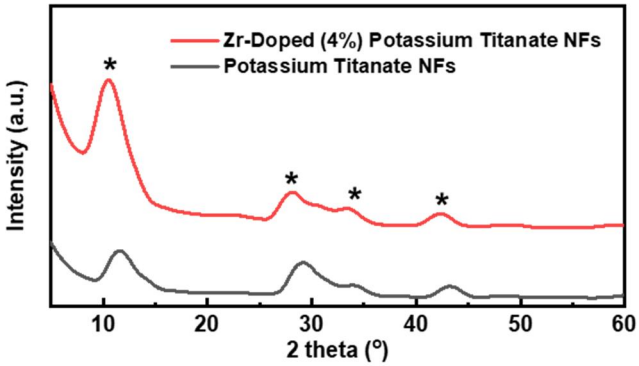


**Figure 3.** X-ray diffraction of zirconium-doped potassium titanate nanofibers.

Comparing the XRD patterns of samples with and without the doping (**Figure 3**), the large Zr-dopant increases the d-space between adjacent titanate sheets by shifting the XRD peak to $d_{(200)}$ = 8.2449 (Å) (or a lower 2-theta angle at 2θ = 10.73°)[31]. This is in contrast with the undoped nanofiber's smaller d-space of $d_{(200)}$ = 7.2449 (Å) at a higher 2-theta angle (2θ = 11.43°). This interlayer spacing expansion is indicative of the optimized lattice doping of the larger $ZrO_6$ octahedron without destroying the titanate lattice structure.

The XRD patterns of potassium titanate nanofibers in undoped and two Zr-doped (2% and 4%) samples are depicted in **Figure 4**. A gradual left-shift of the 200 diffraction with the corresponding d-spacing value increases can be seen. Agreeing with that in the literature, the $Zr^{4+}$ ion doping (i.e., replacing the $Ti^{4+}$) increases the lattice[31,32]. In other words, the 4%-doped sample displays a 2θ value leftward shift, confirming that the overall lattice is being impacted by the $Zr^{4+}$ doping[31,32].

Moreover, the two doped samples XRD patterns show no structural impurities. This is because all the XRD peaks are of the same width and can be indexed to that of potassium titanate, as well as others, including those reported in the literature by our lab[29,30].

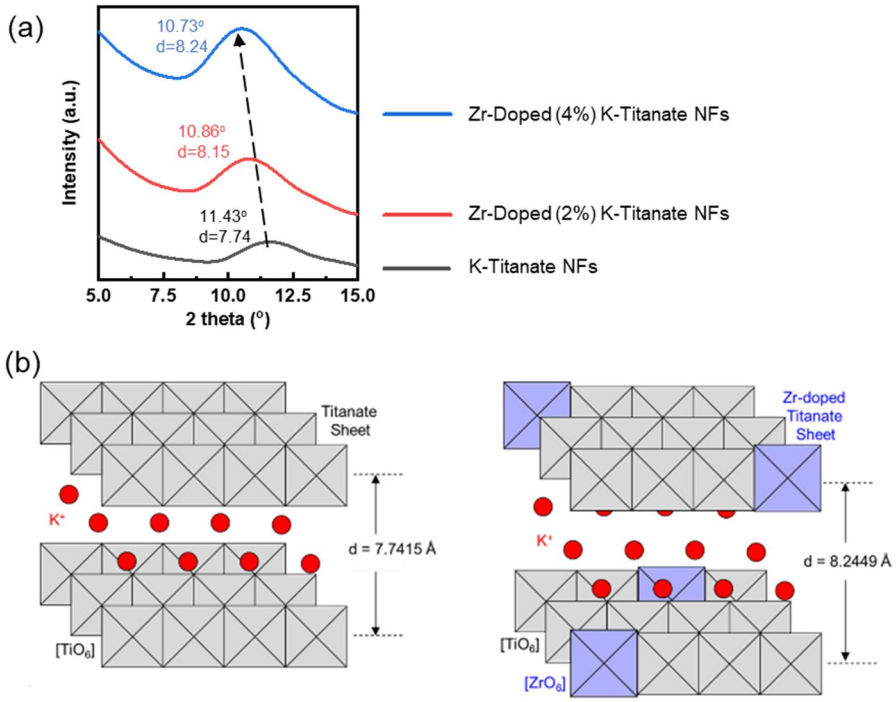


**Figure 4. (a)** Analysis of Zr-doped potassium titanate nanofibers d-space shift; **(b)** Zr-dopant impact on the crystal structure.

The XPS results of potassium titanate confirmed that Zr was successfully doped in 4% K-Zr-Titanate nanofibers (**Figure 5**). The XPS spectra of Zr 3d exhibit two obvious peaks centered at ~180.2 eV and ~182.6 eV, which can be assigned to Zr $3d_{5/2}$ and Zr $3d_{3/2}$, respectively. In addition, another Zr $3d_{5/2}$ and Zr $3d_{3/2}$ slightly shifted to 179.3 eV and 181.3 eV, showing the chemical environments of the Zr-dopant in the nanofibers, probably one for the Zr on the nanofiber surface while the other for the Zr not on the nanofiber surface, which will be verified soon in the follow-up work.

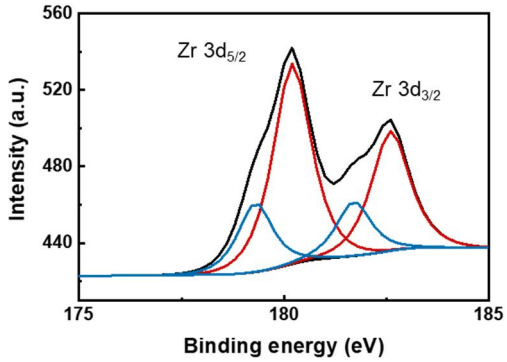


**Figure 5.** XPS spectroscopy of 4% zirconium-doped potassium titanate nanofibers.

Evidently, the $Ti^{4+}$-based $TiO_6$ octahedra in the K-titanate nanofiber's clay-like layered crystal lattice have been partially replaced by the $Zr^{4+}$-based $ZrO_6$ octahedra, which concludes the successful doping of the $Zr^{4+}$, by design. Sterically, the $ZrO_6$ that's larger than the $TiO_6$ would logically stay on the nanofiber surface to minimize the distortion of the nanofiber's $TiO_6$-dominated crystal lattice. Thus-surfaced $ZrO_6$

can potentially help bone-tissue adhesion, as well-established in the literature[27,33,34]. Further, the interlayer $K^+$ cations near the $ZrO_6$ in the K-titanate nanofiber could be more easily (hence more rapidly) replaced by $Ca^{2+}$ cations in body fluid to promote the rapid formation of hydrated calcium phosphates (or hydroxyapatite) on the nanofiber, like other labs reported in the literature using the simulated body fluid (SBF)[18,35]. The strong bonding between the hydroxyapatite coating and the titanate nanofiber substrate surface can chemically secure the bone tissue's long-term strong adhesion to the nanofiber-supported hydroxyapatite, forming an ideal osteogenic/osteoconductive environment[18]. The thus-optimized surface of titanate nanofibers for developing a new bone scaffold can complement other lab methods in promoting the bone scaffold's osteoconductivity[27,33,34,36]. In basic chemistry, this work has demonstrated an innovative and cost-effective method for doping Zr (IV) into the titanate nanofiber lattice, which seems new and important in orthopedic nanomedicine.

## 5. Concluding remarks

Potassium titanate nanofibers doped with zirconium have been successfully fabricated via a simple hydrothermal process, which, to the best of our knowledge, is quite new, especially in orthopedic nanomedicine. The nanofibers' morphology, chemical composition, and crystallinity remained intact after doping, indicating that the hydrothermal process for the crystal framework doping is effective, and the dopant concentrations were controlled well to not negatively impact the nanofiber's lattice structure. This is crucial for maintaining the desired properties of the nanofibers for their intended applications. To assess this material's impact on the bone tissue engineering field, nanofibers of varying Zr-dopant concentrations have been under in vitro investigation for accessing biocompatibility and osteogenic potential.

Logically, the next essential step of investigating these nanofibers with systematically varied Zr-dopant concentrations for biocompatibility and osteogenic potential is currently undergoing. Assessing how these doped nanofibers interact with bone cells will provide valuable insights into these nanofibers' potential as bone implant candidates. Such biocompatibility assessment is a key factor in determining the suitability of materials for medical applications.

One such forward-thinking plan to leverage this work is to dope the titanate nanofibers using, e.g., dual oxide dopants, which may allow for the exploration of a broader range of bone implants with a wide variety of physiological tunability. Understanding the impact of biocompatible transition metals' doping on the physical and chemical properties of the nanofiber-based bone implant is essential for tailoring the biomaterials with respect to every specific application.

Developing a large and new family of doped titanate nanofibers with different compositions and properties is a smart approach to enable researchers to study how variations in doping affect the material's characteristics and performance. This information can be invaluable for optimizing the materials for specific uses in bone tissue engineering or other applications.

## Author contributions

Investigation, PC, YT, ST, MM (Mary Malloy) and LR; writing—original draft preparation, PC, YT and ZRT; writing—review and editing, PC, MM (Micah Maulding), YH and ZRT; funding acquisition, PC, ST, MM (Mary Malloy), LR and ZRT. All authors have read and agreed to the published version of the manuscript.

## Data availability statement

Applicable for reasonable request.

## Funding

This research was funded by the Arkansas State Undergraduate Research Fellowship (SURF)—M.M., University of Arkansas Honors College—L.R., and the Arkansas Biosciences Institute, P.C.

## Acknowledgments

Material characterization assistance was provided by Abayomi Omolewu and Asya Ozkizilcik. The team would like to thank Asya Ozkizilcik for the initial lab training.

## Conflict of interest

The authors declare no conflict of interest. The funders had no role in the design of the study, in the collection, analysis, or interpretation of data, in the writing of the manuscript, or in the decision to publish the results.

## References

1. No YJ, Roohani-Esfahani SI, Zreiqat H. Nanomaterials: The next step in injectable bone cements. *Nanomedicine* 2014; 9(11): 1745–1964. doi: 10.2217/nnm.14.109
2. Zhang B, Li J, He L, et al. Bio-surface coated titanium scaffolds with cancellous bone-like biomimetic structure for enhanced bone tissue regeneration. *Acta Biomaterialia* 2020; 114: 431–448. doi: 10.1016/j.actbio.2020.07.024
3. Min Q, Liu J, Zhang Y, et al. Dual network hydrogels incorporated with bone morphogenic protein-7-loaded hyaluronic acid complex nanoparticles for inducing chondrogenic differentiation of synovium-derived mesenchymal stem cells. *Pharmaceutics* 2020; 12(7): 613. doi: 10.3390/pharmaceutics12070613
4. Wu T, Li B, Wang W, et al. Strontium-substituted hydroxyapatite grown on graphene oxide nanosheet-reinforced chitosan scaffold to promote bone regeneration. *Biomaterial Science* 2020; 8(16): 4603–4615. doi: 10.1039/D0BM00523A
5. Benedini L, Laiuppa J, Santillán G, et al. Antibacterial alginate/nano-hydroxyapatite composites for bone tissue engineering: Assessment of their bioactivity, biocompatibility, and antibacterial activity. *Materials Science and Engineering: C* 2020; 115: 111101. doi: 10.1016/j.msec.2020.111101
6. Oudadesse H, Najem S, Mosbahi S, et al. Development of hybrid scaffold: Bioactive glass nanoparticles/chitosan for tissue engineering applications. *Journal of Biomedical Materials Research Part A* 2020; 109(5): 590–599. doi: 10.1002/jbm.a.37043
7. Mallakpour S, Ramezanzade V. Green fabrication of chitosan/tragacanth gum bionanocomposite films having $TiO_2$@Ag hybrid for bioactivity and antibacterial applications. *International Journal of Biological Macromolecules* 2020; 162: 512–522. doi: 10.1016/j.ijbiomac.2020.06.163
8. Pan H, Gao H, Li Q, et al. Engineered microporous hydrogel scaffolds via pickering emulsions stabilized by MgO nanoparticles promote bone regeneration. *Journal of Materials Chemistry B* 2020; 8(28): 6100–6114. doi: 10.1039/D0TB00901F
9. Nie L, Deng Y, Li P, et al. Hydroxyethyl chitosan-reinforced polyvinyl alcohol/biphasic calcium phosphate hydrogels for bone regeneration. *ACS Omega* 2020; 5(19): 10948–10957. doi: 10.1021/acsomega.0c00727
10. Maji K, Dasgupta S, Bhaskar R, Gupta MK. Photo-crosslinked alginate nano-hydroxyapatite paste for bone tissue engineering. *Biomedical Materials* 2020; 15(5): 055019. doi: 10.1088/1748-605X/ab9551
11. Gao C, Wei D, Yang H, et al. Nanotechnology for treating osteoporotic vertebral fractures. *International Journal of Nanomedicine* 2015; 10: 5139–5157. doi: 10.2147/IJN.S85037
12. Kumar JP, Lakshmi L, Jyothsna V, et al. Synthesis and characterization of diopside particles and their suitability along with chitosan matrix for bone tissue engineering in vitro and in vivo. *Journal of Biomedical Nanotechnology* 2014; 10(6): 970–981. doi: 10.1166/jbn.2014.1808
13. Saravanan S, Vimalraj S, Anuradha D. Chitosan based thermoresponsive hydrogel containing graphene oxide for bone tissue repair. *Biomedicine & Pharmacotherapy* 2018; 107: 908–917. doi: 10.1016/j.biopha.2018.08.072

14. Mohammadi M, Mousavi Shaegh SA, Alibolandi M, et al. Micro and nanotechnologies for bone regeneration: Recent advances and emerging designs. *Journal of Controlled Release* 2018; 274: 35–55. doi: 10.1016/j.jconrel.2018.01.032
15. Aldaadaa A, Al Qaysi M, Georgiou G, et al. Physical properties and biocompatibility effects of doping $SiO_2$ and $TiO_2$ into phosphate-based glass for bone tissue engineering. *Journal of Biomaterials Applications* 2018; 33(2): 271–280. doi: 10.1177/0885328218788832
16. Hashemi A, Ezati M, Mohammadnejad J, et al. Chitosan coating of $TiO_2$ nanotube arrays from improved metformin release and osteoblast differentiation. *International Journal of Nanomedicine* 2020; 15: 4471–4481. doi: 10.2147/iJN.S248927
17. Khan S, Garg M, Chockalingam S, et al. $TiO_2$ doped chitosan/poly (vinyl alcohol) nanocomposite film with enhanced mechanical properties for application in bone tissue regeneration. *International Journal of Biological Macromolecules* 2020; 143: 285–296. doi: 10.1016/j.ijbiomac.2019.11.246
18. Liang F, Zhou L, Wang K. Apatite formation on porous titanium by alkali and heat-treatment. *Surface and Coatings Technology* 2003; 165: 133–139. doi: 10.1016/S0257-8972(02)00735-1
19. Marins NH, Lee BEJ, Silva RM, et al. Niobium pentoxide and hydroxyapatite particle loaded electrospun polycaprolactone/gelatin membranes for bone tissue engineering. *Colloids and Surfaces B: Biointerfaces* 2019; 182: 110386. doi: 10.1016/j.colsurfb.2019.110386
20. Antonini LM, Menezes TL, Santos AGdJ, et al. Osteogenic differentiation of bone marrow-derived mesenchymal stem cells on anodized niobium surface. *Journal of Materials Science: Materials in Medicine* 2019; 30(9): 104. doi: 10.1007/s10856-019-6305-z
21. Hwang C, Park S, Kang IG, et al. Tantalum-coated polylactic acid fibrous membranes for guided bone regeneration. *Materials Science and Engineering: C* 2020; 115: 111112. doi: 10.1016/j.msec.2020.111112
22. Zhang J, Huang D, Liu S, et al. Zirconia toughened hydroxyapatite biocomposite formed by a DLP 3D printing process for potential bone tissue engineering. *Materials Science and Engineering: C* 2019; 105: 110054. doi: 10.1016/jmsec.2019.110054
23. Poon KK, Wurm MC, Evans DM, et al. Biocompatibility of (Ba,Ca) (Zr,Ti)$O_3$ piezoelectric ceramics for bone replacement materials. *Journal of Biomedical Materials Research Part B: Applied Biomaterials* 2020; 108(4): 1295–1303. doi: 10.1002/jbm.b.34477
24. Inui T, Haneda S, Sasaki M, et al. Enhanced chondrogenic differentiation of equine bone marrow-derived mesenchymal stem cells in zirconia microwell substrata. *Research in Veterinary Science* 2019; 125: 345–350. doi: 10.1016/j.rvsc.2019.07.005
25. Soon G, Pingguan-Murphy B, Akbar SA. Modulation of osteoblast behavior on nanopatterned yttria-stabilized zirconia surfaces. *Journal of the Mechanical Behavior of Biomedical Materials* 2017; 68: 26–31. doi: 10.1016/j.jmbbm.2017.01.028
26. Bergemann C, Duske K, Nebe JB, et al. Microstructured zirconia surfaces modulate osteogenic marker genes in human primary osteoblasts. *Journal of Materials Science: Materials in Medicine* 2015; 26: 26. doi: 10.1007/s10856-014-5350-x
27. Cadafalch Gazquez G, Chen H, Veldhuis SA, et al. Flexible yttrium-stabilized zirconia nanofibers offer bioactive cues for osteogenic differentiation of human mesenchymal stromal cells. *ACS Nano* 2016; 10(6): 5789–5799. doi: 10.1021/acsnano.5b08005
28. Frandsen CJ, Brammer KS, Noh K, et al. Tantalum coating on $TiO_2$ nanotubes induces superior rate of matrix mineralization and osteofunctionality in human osteoblasts. *Materials Science and Engineering: C* 2014; 37: 332–341. doi: 10.1016/j.msec.2014.01.014
29. Dong W, Cogbill A, Zhang T, et al. Multifunctional, catalytic nanowire membranes and the membrane-based 3D devices. *The Journal of Physical Chemistry: B* 2006; 110(34): 16819–16822. doi: 10.1021/jp0637633
30. Dong W, Zhang T, Epstein J, et al. Multifunctional nanowire bioscaffolds on titanium. *Chemistry of Materials* 2007; 19(18): 4454–4459. doi: 10.1021/cm070845a
31. Yuan ZY, Zhang XB, Su BL. Moderate hydrothermal synthesis of potassium titanate nanowires. *Applied Physics A—Materials Science & Processing* 2004; 78(7): 1063–1066. doi: 10.1007/s00339-003-2165-x
32. Wang J, Yu Y, Li S, et al. Doping behavior of $Zr^{4+}$ Ions in $Zr^{4+}$-doped $TiO_2$ nanoparticles. *The Journal of Physical Chemistry: C* 2013; 117(51): 27120–27126. doi: 10.1021/jp407662d
33. Alizadeh A, Moztarzadeh F, Ostad SN, et al. Synthesis of calcium phosphate-zirconia scaffold and human endometrial adult stem cells for bone tissue engineering. *Artificial Cells, Nanomedicine, and Biotechnology* 2016; 44(1): 66–73. doi: 10.3109/21691401.2014.909825
34. Sidiqa AN, Hardiansyah A, Chaldun ER, Endro H. Preparation and characterization of zirconium oxide-doped hydroxyapatite. *Key Engineering Materials* 2019; 829: 54–59. doi: 10.4028/www.scientific.net/kem.829.54
35. Wang X, Liu SJ, Qi YM, et al. Behavior of potassium titanate whisker in simulated body fluid. *Materials Letters* 2014; 135: 139–42. doi: 10.1016/j.matlet.2014.07.145

36. Kokubo T, Yamaguchi S. Novel bioactive titanate layers formed on Ti metal and its alloys by chemical treatments. *Materials* 2009; 3(1): 48–63. doi: 10.3390/ma3010048